J Sol-Gel Sci Technol (2016) 80:881–892
DOI 10.1007/s10971-016-4173-2

ORIGINAL PAPER: SOL-GEL, HYBRIDS AND SOLUTION CHEMISTRIES

Effect of heat treatment on the crystalline structure and hydrophilic properties of TiO_2 porous thin films

Yanwen Zhang[1] · Moo-Chin Wang[2] · Huiting He[1] · Hong Li[1]

Received: 6 January 2016 / Accepted: 26 July 2016 / Published online: 1 August 2016

Abstract TiO_2 porous thin films have been synthesized successfully using tetrabutyl titanate ($Ti(OC_4H_9)_4$, $Ti(OBu)_4$) as the initial material, with acetylacetone (AcAc) and diethanolamine (DEA) as the complexing agents, prepared by a sol–gel spin-coating process. The effect of heat treatment on the crystalline structure and hydrophilic properties of TiO_2 porous thin films has been studied by X-ray diffraction, Fourier transform infrared spectra, field emission scanning electron microscopy, and water contact angles (WCAs) apparatus. It was found that the TiO_2 porous thin films showed hydrophobicity before annealing and after annealing at temperatures below 300 °C for 60 min. Otherwise, the TiO_2 porous thin films exhibited a natural superhydrophilic property with the WCAs <5° when annealed at temperature higher than 450 °C for 30 min and without UV irradiation. The natural hydrophilic property of TiO_2 porous thin films was independent on the microstructure and morphology but depended on crystal structure after heat treatment.

✉ Moo-Chin Wang
mcwang@kmu.edu.tw

✉ Hong Li
lh_648@whut.edu.cn

[1] State Key Laboratory of Silicate Materials for Architectures, Wuhan University of Technology, Wuhan 430070, China

[2] Department of Fragrance and Cosmetic Science, Kaohsiung Medical University, 100 Shih-Chuan 1st Road, Kaohsiung 80708, Taiwan

Graphical Abstract

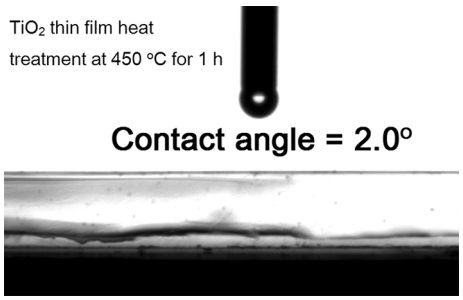

Keywords Heat treatment · Anatase TiO_2 · Porous thin films · Hydrophilic property · Water contact angles (WCAs)

1 Introduction

Superhydrophilic titanium dioxide (TiO_2) thin films have been applied in various fields, such as for biomedical applications [1], antireflection and antifogging [2, 3], antimicrobial activities [4], and self-cleaning [2, 5], owing to TiO_2 thin films possessing hydrophilic, chemical, and outstanding optical properties. Anatase TiO_2, with an energy band of about 3.2 eV, which causes the superhydrophilicity of TiO_2 thin films, vanishes rapidly without ultraviolet (UV) light irradiation, meaning that the current applications of TiO_2 thin films are limited mainly to outdoor use [6, 7].

When the TiO_2 thin films are treated with a given chemical composition to increase the surface roughness, this can render the thin films more hydrophobic or hydrophilic. Therefore, porous TiO_2 thin films can enhance the

surface roughness. Porous TiO_2 thin films have been fabricated by various processes such as the sol–gel method [5, 8–10], sol–gel and evaporation-induced self-assembly [11], sputtering techniques [12], direct deposition from aqueous solutions [13], spray pyrolysis deposition technique [14], and template hydrothermal synthesis [15]. Among these processes, the sol–gel process is an important method for fabricating the porous TiO_2 thin films, because it possesses a number of advantages, such as the atomic-scale mixing of constituents, easy operation, and cost factor [16].

Transparent, nanosized, crystalline TiO_2 thin films with high photocatalytic activity, fabricated on soda-lime glass substrates, using the TiO_2 sol solution prepared by the sol–gel process, have been reported by Yu et al. [9]. They demonstrated that the TiO_2 gel films were converted to anatase TiO_2 thin films with the highest photocatalytic activity when the TiO_2 gel films had been heat-treated at 500 °C. Zhao et al. [5] pointed out a new method for enhancing the photocatalytic activity of TiO_2 thin films, when the thin films were directly coated on the soda-lime glass, prepared by the sol–gel process, and the films were treated in an acidic solution. In addition, Wang et al. [11] pointed out that the mesostructured TiO_2 thin films were fabricated by the sol–gel and evaporation-induced self-assembly processes, using the triblock copolymer Pluronic F127 ($EO_{106}PO_{70}EO_{106}$) as the templating agent and ($Ti(OC_4H_9)_4$, $Ti(OBu)_4$) as the titanium source. They also reveal that the as-synthesized mesoporous TiO_2 thin films have excellent thermal stability and possess pores with a diameter larger than 7 nm, with a narrow pore size distribution, and thick inorganic walls composed of nanocrystalline anatase.

On the other hand, the effect of ultrasonic treatment on the surface of highly hydrophilic TiO_2 was reported by Sakai et al. [17]. They reveal that the contact angle of surface hydrophilicity decreased to approximately 11° when the pure water was added after ultrasonic treatment. Watanabe et al. [18] studied the single-crystal structure of rutile and polycrystalline anatase TiO_2 dependence on the photoinduced hydrophilic conversion and pointed out that the wettability conversion rate of the surface with the bridging oxygen site is low, compared to that without the bridging site. Moreover, the relationship between the natural superhydrophilic and structurally porous TiO_2 thin films has also been reported by various researchers [19–22]. However, the effect of heat treatment on the crystalline structure and superhydrophilic properties of TiO_2 porous thin films without ultraviolet (UV) light irradiation has not been discussed in detail.

In the present study, the porous TiO_2 thin films were synthesized using acetylacetone (AcAc) and diethanolamine (DEA) as complexing agents, prepared by a sol–gel spin-coating process. The aim of the present work was to: (1) study the effect of heat treatment on the crystalline structure of TiO_2 powders and thin films; (2) observe the morphologies of TiO_2 thin films before and after heat treatment; and (3) evaluate the effect of heat treatment on the superhydrophilic properties of TiO_2 thin films.

2 Experimental procedure

2.1 Materials

In the present study, tetrabutyl titanate ($Ti(OBu)_4$) ($Ti(OC_4H_9)_4$, purity >98.0 %), absolute ethanol (C_2H_5OH, purity >99.7 %), acetylacetone (AcAc) ($C_5H_8O_2$, purity >99.0 %), diethanolamine (DEA) ($C_4H_{11}NO_2$, purity >98.0 %), and nitric acid (HNO_3, purity ≥65–68 %) were used as the initial materials. All initial materials were supplied by Sinopharm Chemical Reagent Co. Ltd., China. The soda-lime silicate glasses with a dimension of 2.5 cm × 2.5 cm × 0.1 cm were used as the substrates.

2.2 Preparation of TiO_2 thin films

The TiO_2 thin films were prepared using sol–gel spin-coating on soda-lime silicate glass substrates, according to the chart shown in Fig. 1 [23]. The "A" solution was made by $Ti(OBu)_4$, absolute ethanol, AcAc, and DEA in volumes of 10, 27, 2, and 2 ml, respectively. The "B" solution was made by mixing absolute ethanol, deionized water, and HNO_3 in volumes of 53, 10, and 1 ml, respectively. The sol–gel of TiO_2 was prepared by sequentially premixing the "B" solution into the "A" solution and stirring at room temperature for 10 min to form sol 1. Then, sol 1 was stirred at room temperature for 90 min to form an insoluble gel. The gel was then aged at room temperature for 24 h.

Before spin-coating, the soda-lime silicate glass substrates with a dimension of 7.5 cm × 2.5 cm × 0.1 cm were degreased, cleaned thoroughly, and dried in an oven at 80 °C for 30 min. First, the gel was spin-coated on the substrate once with a screw rotation rate of 750 rpm for 15 s and subsequently at 5000 rpm for 30 s. Then, the films were dried at 105 °C for 30 min. In order to heat-treat the dried sample, it was transferred to another electric furnace at heating rates of 5 °C/min to 200, 300, 350, 400, 450, 500, and 550 °C, respectively, in air for 60 min. Then, porous TiO_2 thin films were obtained. Moreover, the dried samples were also heat-treated at 450 °C for 10, 30, and 120 min, respectively. In order to compare the developed phase, the titanium oxide gels were also directly dried, and

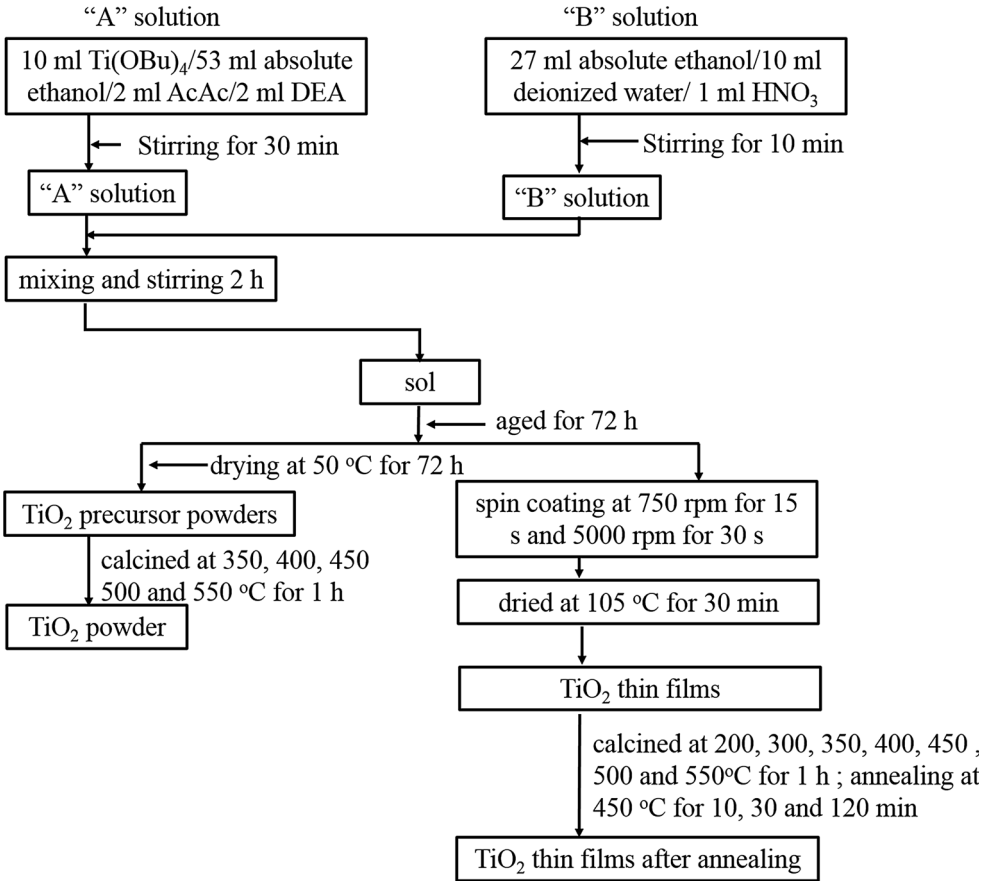

Fig. 1 Flowchart for preparing TiO_2 thin films

calcined between 300 and 550 °C for 1 h. Then, the TiO_2 powders were obtained.

2.3 Sample characterization

The crystalline phase of TiO_2 powders and TiO_2 thin films was identified by X-ray diffraction (XRD, D8 Advance, Germany), with a CuK_α target and an Ni filter, operated at 30 kV, 200 mA, and a scanning rate (2θ) of 1°/min. The morphologies of the surface and cross section of the TiO_2 thin films were observed by field emission scanning electron microscopy (FESEM, Zeiss Ultra Plus, Germany). The Fourier transform infrared spectra of TiO_2 sols spread on KBr pellets were recorded on a Fu Liye transform infrared spectrometer (FTIR, Nicolet6700, America), with 0.019 cm^{-1} resolution in the frequency range from 4000 to 400 cm^{-1}. The water contact angles (WCAs) of TiO_2 thin films without UV irradiation were measured at ambient temperature, by an automatic contact angle measuring device (Dataphysics OCA35, Germany). Water droplets were generated automatically, with a volume of 5 µl. Samples were kept in a dark box for 48 h before the measurement of WCAs. Typically, the average value of measurements at five different positions of the TiO_2 thin films' surface was adopted as the value of the WCAs.

3 Results and discussion

3.1 FTIR analysis of TiO_2 sols

Figure 2a shows the FTIR spectrum of TiO_2 sols prepared by using $Ti(OBu)_4$, absolute ethanol, AcAc, and DEA as the initial materials, where the OH flexion bands face out

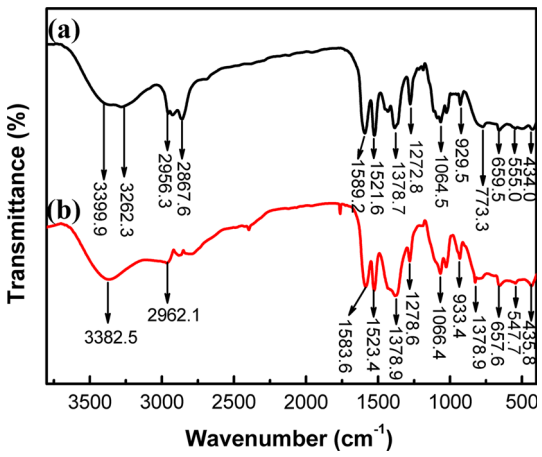

Fig. 2 FTIR spectrum of TiO_2 sols prepared by using: *a* $Ti(OC_4H_9)_4$, absolute ethanol, AcAc, DEA and *b* $Ti(OC_4H_9)_4$, absolute ethanol, AcAc, DEA, HNO_3, and deionized water

and the low-energy band of 435.8 cm^{-1} appear due to a stretching vibration of Ti–O band in titania [24]. The weak absorption peak is seen at 659.5 cm^{-1} because of the hydrolysis and polycondensation reaction of –(Ti–O)–n [25]. The Ti–O bond bands are found at 555.0 and 773.3 cm^{-1} of the low-energy interval, and a well-defined band typical of hydroxyl groups (≡Ti–OH) is found at 929.5 cm^{-1} [24]. The weak absorption peak to be found at 1064.5 cm^{-1} is attributed to the stretching vibration of C–O band [26]. The absorption peak at 1272.8 cm^{-1} is attributed to the asymmetric vibration of C–O [27, 28]. The absorption peaks at 1378.7 and 1432.9 cm^{-1} are due to the symmetric band of α-CH_3 [29] and symmetric stretching vibration of CH_3 [27, 29]. Two absorption peaks at 1521.6 and 1589.2 cm^{-1} are due to the acetylacetonate groups bound to titanium [25]. The C–H stretching vibration of –CH_2– and –CH_3– is found at 3262.3 and 3399.4 cm^{-1}, respectively, which is caused by the OH stretching band [24, 25].

The FTIR spectrum of TiO_2 sols prepared by using $Ti(OC_4H_9)_4$, absolute ethanol, AcAc, DEA, HNO_3, and deionized water as initial materials is shown in Fig. 2b. It is seen that the result of Fig. 2b is similar to that of Fig. 2a, except the peaks at 2867.6 and 3262.3 cm^{-1} disappear in Fig. 2b.

3.2 Crystalline structure of the TiO_2 powder and TiO_2 thin films

Figure 3 shows the XRD patterns of TiO_2 precursor films after being calcined at various temperatures for 1 h. The XRD patterns of the TiO_2 precursor powders, after calcination at 300 and 350 °C, are shown in Fig. 3a, b, respectively, which reveals that the powders still maintained the amorphous state. Figure 3c, d shows the XRD patterns of the TiO_2 precursor after being calcined at 400 and 450 °C for 1 h, respectively, which indicates that the powders only have a single phase of anatase TiO_2, due to the reflections of (101), (004), (200), (105), (211), (204), (116), (220), and (215) of anatase TiO_2 (JCPDS Cards: 89-4921). However, Fig. 3c also reveals that the broad and weak intensities of the peak are a result of the fine crystals in the nanometer-to-submicron-meter range and/or the poor crystallinity of anatase TiO_2 [30, 31]. Figure 3e, f shows the XRD patterns of the TiO_2 precursor powders after being calcined at 500 and 550 °C for 1 h, respectively, which reveals that the patterns still maintained the single phase of anatase TiO_2. It is also found that the intensity of the reflection peaks was greater than the corresponding peaks, as shown in Fig. 3d. This result was attributed to the crystallinity, and the size of the anatase TiO_2 crystalline increased as the calcination temperature rose from 450 to 550 °C.

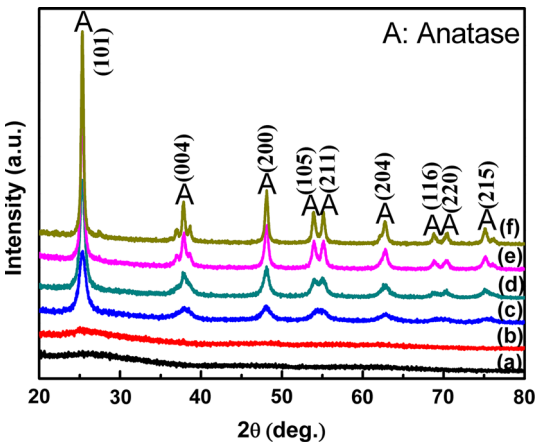

Fig. 3 XRD patterns of TiO_2 powder samples calcined at various temperatures for 1 h: *a* 300 °C; *b* 350 °C; *c* 400 °C; *d* 450 °C; *e* 500 °C; and *f* 550 °C (A: anatase TiO_2)

High-purity and spherical nanocrystalline anatase TiO_2 is synthesized by a modified sol–gel process, using anhydrous $TiCl_4$ mixed with ethanol at 0 °C. Li et al. [32] reported that a yellowish sol was first obtained and then transformed into the phase of anatase TiO_2 when baked at 87 °C for 3 days. They also pointed out that while heating the powders after baking between 87 and 600 °C for 2 h, the powders still maintained the phase of anatase TiO_2. Katoch et al. [33] demonstrated that nanocrystalline anatase TiO_2 is dispersed uniformly in the stable sol using the processes of hydrolysis and condensation of titanium isopropoxide in ethanol, with HNO_3. The results of the present study were in agreement with previous results [26, 27].

Yeh et al. [34] reported the use of titanium tetrachloride ($TiCl_4$) as the initial material for preparing TiO_2 nanocrystallines using a coprecipitation process and pointed out that when the precursor powders had been calcined at temperatures between 200 and 400 °C for 2 h, the calcined powders only contained single phase of anatase TiO_2. After being calcined at 500 °C for 2 h, the XRD pattern shows that anatase TiO_2 and rutile TiO_2 coexist. Yeh et al. [35] also synthesized mesoporous TiO_2 nanocrystalline powder by a simple coprecipitation process, without adding surfactant, and demonstrated that the XRD pattern shows that anatase TiO_2 and type II NH_4Cl coexist when the TiO_2 precursor powders had been calcined at 300 °C for 2 h. In addition, the XRD pattern shows that the calcined powders only contained a single phase of anatase TiO_2 when the precursor powders have been calcined at 400 °C for 2 h. The results of Yeh et al. [34, 35] are only in partial agreement with the present study. The difference between the present study and previous works was due to the different initial materials and synthesis process.

The anatase TiO_2 is thermodynamically less stable than the rutile TiO_2. Therefore, the phase transformation from

the anatase to rutile TiO_2 occurs at an elevated temperature. Liao et al. [36] pointed out that the Gibb's free energy (ΔG) transformation from anatase (A) to rutile (R) TiO_2 is expressed as:

$$\begin{aligned}\Delta G_{A\to R} = {} & 2374.3 + 0.8569\,T - 1.524\,T\ln T \\ & - 1.89\times 10^{-3}T + 1.43\times 10^{-7}T^{-1} \\ & + 1.1\times 10^{-7}T^{3} + 305.525\sqrt{T}\end{aligned} \quad (1)$$

At 500 °C, the value of $\Delta G_{A\to R}$ is 3.9×10^3 kJ/mol [23]. Because the value of $\Delta G_{A\to R}$ at 500 °C is positive, the phase from anatase to rutile TiO_2 can be considered as a movement from a stable state to a metastable state. This result means that the rutile TiO_2 was not visible in the present study. Moreover, the energy of 3.9×10^3 kJ/mol can be considered as the driving force for the rutile nucleation that occurred [37].

The XRD patterns of TiO_2 thin films prepared by spin-coating after being calcined in air at various temperatures for 1 h are shown in Fig. 4. Figure 4a–c shows the XRD patterns of the thin films after being calcined at temperatures between 300 and 400 °C, which reveals that the thin films are in the amorphous state. This result is almost fully in agreement with the results of Fig. 3a–c. Figure 4d–f shows the XRD patterns of thin films after being calcined at a temperature between 450 and 550 °C and reveals that only (101) the peak of the anatase TiO_2 appeared. However, the intensity of the (101) peak increased slightly with an increase in the calcined temperature, but was still weak and broad due to poor crystallinity and small crystals in the submicron-meter -to-nanometer scale [30, 31].

The use of titanium isopropoxide (TTiP), absolute ethanol, and acetone as initial materials for fabricating TiO_2 thin films prepared by sol–gel spin-coating has been reported [23, 38, 39]. These studies have pointed out that the TiO_2 thin films only contained single phase of anatase

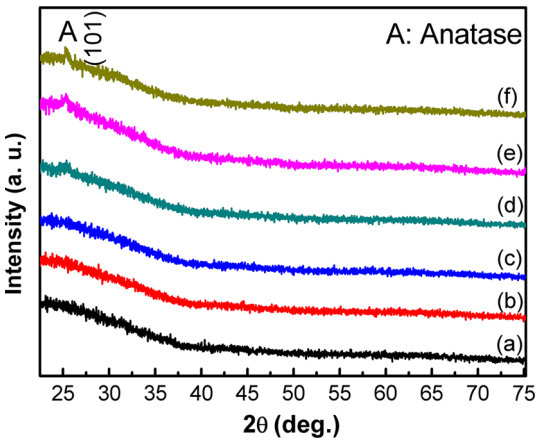

Fig. 4 XRD patterns of porous films after being calcined at different temperatures for 1 h: *a* 300 °C; *b* 350 °C; *c* 400 °C; *d* 450 °C; *e* 500 °C; and *f* 550 °C (A: anatase TiO_2)

TiO_2 when the as-coated thin films had been calcined at 500 °C for 1 h. These results are in agreement with the present study. When the TiO_2 thin films with a thickness of <0.5 μm had been calcined at 520 °C for 1 h, the XRD patterns show that the phase formation is either brookite TiO_2 or sodium titanate ($Na_2O{\cdot}xTiO_2$), due to the reaction of Na_2O migration from the soda-lime glass substrate to TiO_2 thin films [8, 40]. However, the XRD patterns show the obvious diffraction peaks of anatase TiO_2 with some preferred orientation of anatase (101) when the thickness of TiO_2 thin films is >0.5 μm, after being calcined at 520 °C for 1 h [8]. This result was partially in agreement with the present study.

3.3 Microstructure and morphology of the TiO_2 thin films before and after heat treatment

The cross-sectional FESEM microstructures of TiO_2 thin films before and after heat treatment at various temperatures for 1 h are shown in Fig. 5. Figure 5a shows the cross-sectional microstructure of TiO_2 thin films before heat treatment, which reveals that the thickness of thin films is about 381.8 ± 49.6 nm, but the thickness distribution was not uniform. Moreover, a pore exists in the interior of thin films, which was speculated that the air dissolved in film while spin-coating. Figure 5b–c shows the TiO_2 thin films after heat treatment at 300–450 °C for 1 h. Figure 5a shows that the thickness of thin films decreases from 381.8 ± 49.6 to 204.0 ± 17.5 nm from before to after heat treatment at 450 °C. This phenomenon is attributed to the volatility amount of organic solvent and H_2O increases with increasing heat treatment temperature, which leads to enhance the films densification and decrease the thickness of thin films.

The FESEM microstructures of the TiO_2 thin films before and after heat treatment in air at various temperatures for 1 h are shown in Fig. 6. Figure 6a shows the obvious macropores thin films before heat treatment with an average size around 3.32 μm. This result is due to the phase separation that is occurred in the course of condensation. Figure 6b shows the microstructure of TiO_2 pore thin films after heat treatment at 300 °C for 1 h, which reveals the thin films with an average pore size of about 3.66 μm. The pore size of TiO_2 thin films before heat treatment was smaller than after heat treatment, and this is due to the removal of solvents leading to pore size increase. This result also shows that the pore size of TiO_2 thin films is affected by the heat treatment temperature. Moreover, Fig. 6c, d shows the TiO_2 pore thin films with an average size approximately 3.67 and 3.64 μm after heat treatment at 400 and 450 °C for 1 h, respectively. The results are similar to Fig. 6b due to solvent of ethanol evaporated completely.

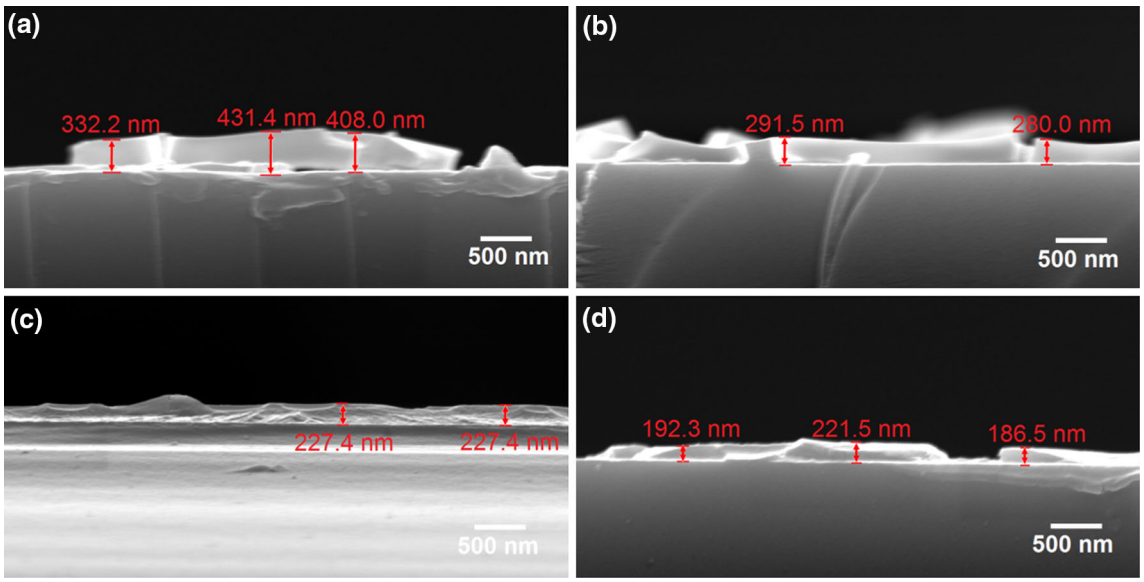

Fig. 5 Cross-sectional FESEM microstructures of TiO_2 thin films before and heat treatment at various temperatures for 1 h: **a** before; **b** 300 °C; **c** 400 °C; and **d** 450 °C

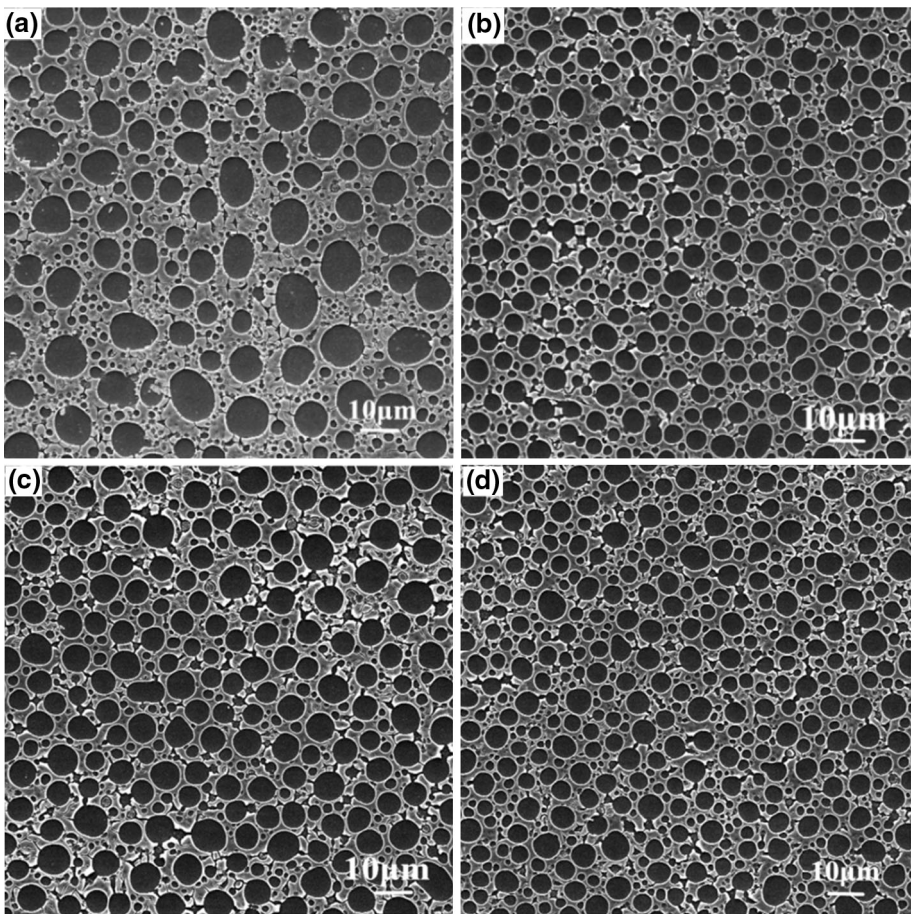

Fig. 6 FESEM microstructures of TiO_2 thin films before and heat treatment at different temperatures for 1 h: **a** before; **b** 300 °C; **c** 400 °C; and **d** 450 °C

Figure 7 shows the relationship between relative amount of pores and pore size for TiO_2 thin films before and after heat treatment at various temperatures for 1 h. It is found that the pore size of the thin films before heat treatment decreased with increasing heat treatment temperature. This result is due to the Ti^{4+} oligomers that are rapidly formed

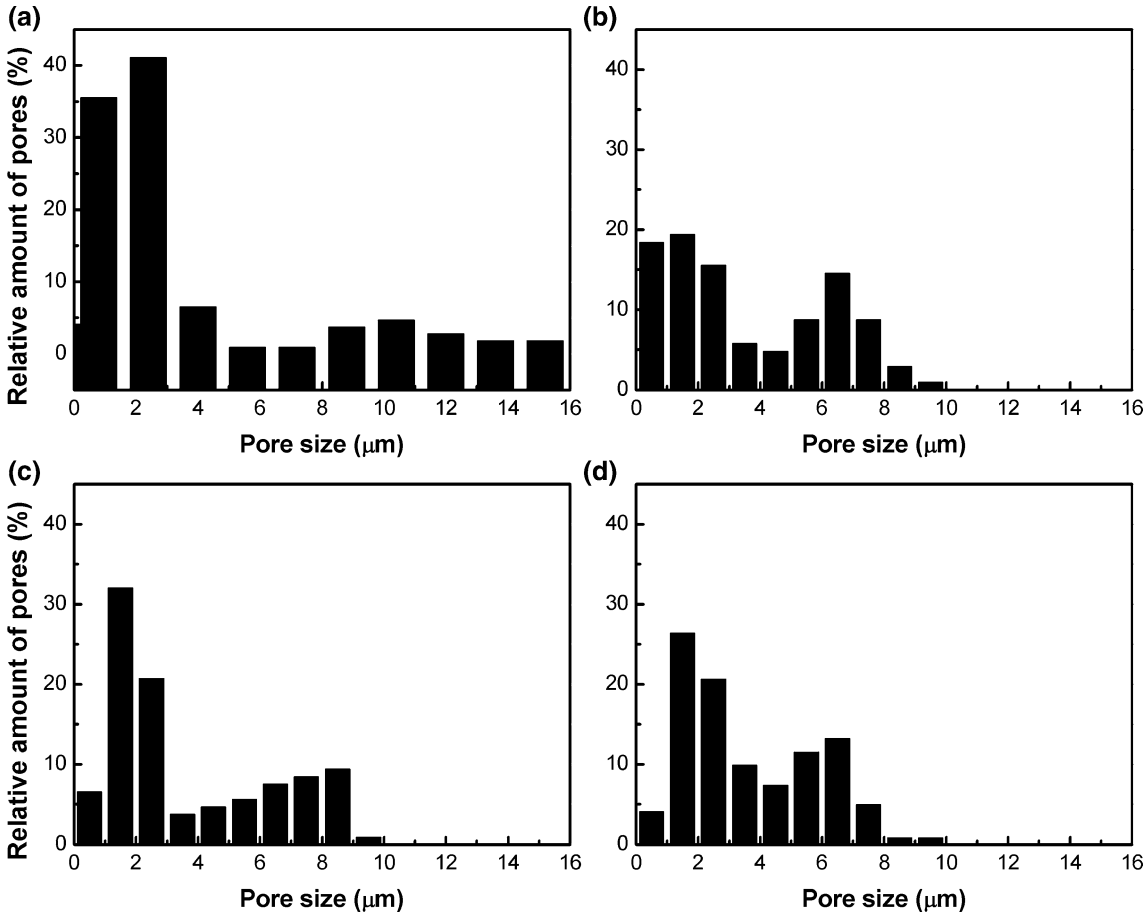

Fig. 7 Effect of heat treatment temperature on the relative pore size distribution of TiO_2 pore thin films: **a** before heat treatment; **b** 300 °C; **c** 400 °C; and **d** 450 °C

at a certain pH condition increasing the comparability to low degree and phase separation [25, 41]. In the polycondensation process, phase separation occurred by the reduction in miscibility between the polar solvent and polycondensed inorganic species [25], and As the polarity of solvents decreased, the polarity gap between solvent and gel phase reduced, leading to the reduction in the rate of phase separation and the pore size becoming smaller with increase in the heat treatment temperature.

In the present study, AcAc and DEA were used as complexing agents simultaneously. Huang et al. [25] have pointed out that the isolated or interconnected pores were formed because phase separation occurred in the sol–gel process in the presence of AcAc and DEA. Figure 6 shows the isolated or interconnected macropores with an average size greater than 3.0 μm in TiO_2 surface because of the presence of AcAc and DEA agents [25]. These two complexing agents have been used as an effective addition for controlling the rate of hydrolysis and precipitation in the sol–gel process for metal alkoxides through complexing reaction [25]. The AcAc displays a stronger chelate-forming ability with the $Ti(OBu)_4$ precursor, which leads to decreases in the rate of hydrolysis and precipitation of the $Ti(OBu)_4$ precursor [42]. DEA possessing the hydrogen bonding is used as a highly polar solvent, and it was hydrolyzed to produce ammonia in the presence of HNO_3 [43]. While mixing DEA with strong acid, the pH changes, accelerating the polycondensation stage of TiO_2 oligomers. The polarity of the gel phase slightly decreases when the dehydration and debutanation polycondensation occurred, leading to the consumption of hydroxyl groups, while the polarity of the solvent is still high [43]. The pore size becomes smaller with the same amount of acid and base reported by Huang et al. [25]. In the present study, the gels were completely miscible before adding HNO_3 to organic compounds. Adding HNO_3 to the weak alkaline DEA accelerates the polycondensation reaction of TiO_2 oligomers and eventually induces the sol–gel transition. The schematic diagram of the phase separation process of adding HNO_3 is shown in Fig. 8. In the polycondensation process, the reduction in miscibility between the polycondensed inorganic species and polar solvent decreases leads to a phase separation [41, 44]. Malfatti et al. [45] suggested that directly using propylene glycol (PPG) triggers

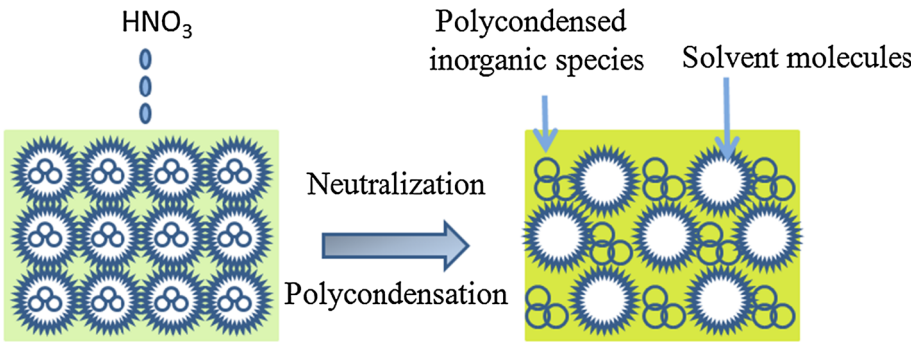

Fig. 8 Schematic diagram of the phase separation process after adding HNO_3

demixing. The difference between the mechanisms of phase separation was due to the different initial materials.

The various sol–gel systems on the basis of polymerization-induced phase separation have been successfully used for designing and fabricating the well-defined macroporous monoliths [41, 46]. Chen et al. [47] used the sol–gel process for preparing the ZnO/TiO_2 thin films and pointed out that the polymerization-induced phase separation leads to the formation of porous structure.

On the other hand, the time of the onset of phase separation relative to the sol–gel transition was adjusted, and then the size of the macropores can be controlled due to the domain formation when the phase separation involves a coarsening process. The pore size control was readily accomplished through only a change in the starting composition [41]. The sol–gel method that accompanied phase separation is one of the promising techniques for fabricating monolithic materials with a bimodal pore structure [41, 48].

In order to control the bicontinuous morphology of macroporous in the present study, the following three key points must be attained. The first key point is the use of $Ti(OBu)_4$ as TiO_2 precursor leading to the reactivity of decreasing polycondensation [41]. Moreover, the complexing agent AcAc is used to reduce the reactivity of $Ti(OBu)_4$ polycondensation for controlling the rate of hydrolysis and precipitation of metal alkoxides [25, 42, 49]. The second key point is the control of the pH of synthetic system [25]. HNO_3 is used as the strong acid catalyst, which also reduces the reactivity of $Ti(OBu)_4$ to H_2O [41]. The third key point was the use of DEA in the present study which can promote the control over the rate of condensation and effectively cause the phase separation [41]. Moreover, in order to understand the mechanism of pore formation, Huang et al. [25] also pointed out that due to the composition difference between the phases and domains continues to enhance. Therefore, the phase size also started to increase that was strongly governed by the surface energy [48].

On the other hand, since the thin films of present study were obtained by a sol–gel spin-coating process, an evaporation-induced gelation causes rapid solidification of the developing domains in the coated layer. This rapid freezing transient structure created the two-dimensionally phase-separated structure on a substrate [43]. When the gel was spin-coated on the substrate, the micropores formed after evaporation drying [48]. In addition, when the domains of solvent phase were dispelled from the substrate, the unoccupied regions formed, whereas the porous skelecton formed due to the domains of gel phase spread on the substrate surface. This result leads to the pore segregation in the surface of thin films [43, 50].

The macropores were distributed sharply, and the pore size decreased with increasing molar ratio of H_2O to $Ti(OBu)_4$ in the starting composition [41]. In the system with a larger amount of H_2O, the hydrolysis reaction of titanium alkoxide was more strongly promoted to enhance the number of hydroxyl groups on the surface of the TiO_2 oligomers. Therefore, the compatibility of the two-size distribution of pores increased in the thin films. The increase in amount of H_2O makes the phase separation tendency become weaker, and a finer bicontinuous structure is obtained as a result of the later onset of phase separation, the small pores being left behind after evaporation drying, as reported by Konishi et al. [41].

However, Bu et al. [42] noted a pore size in the range of 200–500 nm for the sol at a molar ratio of $H_2O/Ti(OBu)_4 = 1$ with triethanolamine (TEA). This result was not in agreement with the present study, owing to the molar ratio of $H_2O/Ti(OBu)_4$ in the present study being 19.2, which was greater than that reported by Bu et al. [42]. Moreover, the starting composition of the present study used the DEA and AcAc as the complexing agents. On the other hand, the phase separation occurred much earlier than the gelation, leading to bicontinuous structure fragments changing into spherical particles to reduce the interfacial energy when the molar ratio of $H_2O/Ti(OBu)_4$ was smaller than 20.75, as reported by Konishi et al. [41]. This result was not in agreement with the present study because of the different initial materials and the composition of the sol.

3.4 Hydrophilic properties of porous TiO_2 thin films

The surface wettability of the porous TiO_2 thin films after heat treatment at different temperatures for 1 h, and heat treatment at the same temperature for various holding times, was investigated by measuring the water contact angles (WCAs) on the surface of the thin films. The optical images of water spreading on the surface of porous TiO_2 thin films after heat treatment at different temperatures for 1 h are shown in Fig. 9. After heat treatment at 300 °C, the contact angle (CA) of water spreading on the surface of porous TiO_2 thin films was 97.4°, as shown in Fig. 9a. The figure reveals that the surface of porous TiO_2 thin films has a hydrophobic property. The optical image of water spreading on the surface of porous TiO_2 thin films after heat treatment at 350 °C for 1 h is shown in Fig. 9b, which reveals that the CA was 64.7°; thus, the films are both hydrophobic and hydrophilic. After heat treatment at 400 °C for 1 h, the optical image of water spreading on the porous TiO_2 thin films shows that the CA was 9.2°, as shown in Fig. 9c, which reveals the hydrophilic property. Figure 9d shows the image of water spreading on the surface of porous TiO_2 thin films after heat treatment at 450 °C for 1 h and demonstrates that the CA was 2.0°. Therefore, the surface of porous TiO_2 thin films has a superhydrophilic property. The results of Fig. 9 also show that the wetting ability of porous TiO_2 thin films gradually transits from hydrophobic to superhydrophilic with a rise in the calcined temperature, from 300 to 450 °C. In the report of Wenzel [51], it is well established that for a given chemical composition to increase the roughness of a surface can render it more hydrophobic or more hydrophilic. The introduction of porosity to the surface makes hydrophobic amorphous TiO_2 films, and hydrophilic crystalline TiO_2 films exhibit better hydrophobicity and hydrophilicity, respectively.

The water contact angles of the porous TiO_2 thin films, before and after heat treatment, at temperatures between 200 and 450 °C for 1 h, are listed in Table 1. It can be seen that the contact angle is more than 90° or less than 5° when the calcined temperatures were lower, 300 °C, or higher, 450 °C, respectively. As shown in Fig. 6, the microstructure and morphology of TiO_2 pore thin films were different before and after heat treatment in air at 300 °C for 1 h. However, the water contact angles of the porous TiO_2 thin films maintained substantially, and no other changes can be detected. In addition, the microstructure and morphology of films have influenced by heat treatment process while annealing over 300 °C for 1 h; however, the water contact angles of the porous TiO_2 thin films decreased, indicating that the natural hydrophilic property of TiO_2 porous thin films depended on the microstructure and morphology, but the surface of TiO_2 thin films with amorphous and crystalline anatase TiO_2 led to the above-mentioned results. Wenzel [44] also pointed out that the wettability of the rough surface is greater than that of the smooth surface. However, the results of Figs. 6 and 7 show that after heat treatment, the porous TiO_2 thin films have different microstructures and pore sizes. Therefore, the difference of water contact angles of the porous TiO_2 thin films after heat treatment at temperature lower than 300 °C and higher than 450 °C can be attributed to the surface with an amorphous and crystalline state. Moreover, Wang et al. [52] noted that oxygen adsorption of the TiO_2 thin film surface becomes greater, leading to the surface

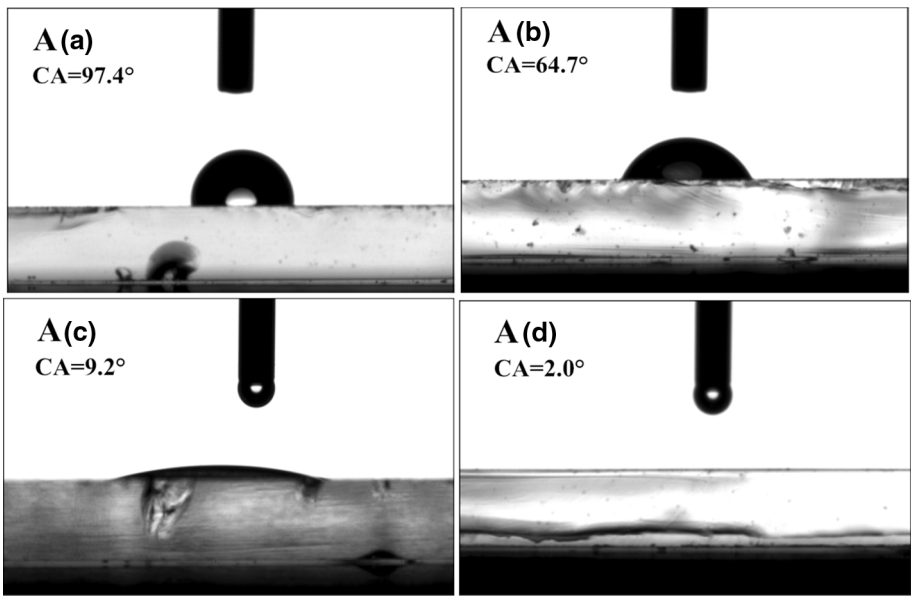

Fig. 9 Optical images of water spreading on TiO_2 porous films after heat treatment at different temperatures for 1 h: **a** 300 °C; **b** 350 °C; **c** 400 °C; and **d** 450 °C

Table 1 WCAs of the TiO_2 films on glass substrates before annealing at various temperatures for 1 h

Annealing temperature (°C)	Before annealing	200	300	350	400	450
Equilibrium WCA (°)	96.8	98.5	97.4	64.7	9.2	2.0

wettability quickly reconverting from hydrophilicity to hydrophobicity.

Figure 10 shows the dependence of the contact angle on the heat treatment temperature and wetting times for a water droplet added to the surface. It was seen that the porous TiO_2 thin films show the hydrophobic property when the thin films have been heat-treated at 300 °C for 1 h, due to the surface with the amorphous state. In addition, Fig. 10 also shows that the water contact angle decreased rapidly with the wetting time for a water droplet added to the surface with a rise in the heat treatment temperature. However, the water contact angle decreased and was saturated at 9.2° and 2.0°, when the porous TiO_2 thin films had been calcined at 400 and 450 °C for 1 h, respectively. This result occurred because the various calcined temperatures created different surfaces of porous TiO_2 thin films.

Wang et al. [52] pointed out that the water contact angle rapidly decreased with the illumination time of ultraviolet irradiation because the (110) and (100) reflections indicate that defects can be relatively easily produced on the (110) and (100) reflections, and the surface wettability conversion of TiO_2 greatly depends on the amount of light-induced defect sites that are relevant to the surface structure of TiO_2 single crystal. However, the porous TiO_2 thin films of the present study were observed without ultraviolet light irradiation. The behavior with decreased water contact was similar to the reported results of Wang et al. [52]. Therefore, it can be speculated that the effect of heat treatment temperatures on the surface structure of porous TiO_2 thin films, calcined at higher temperature, is similar to the larger amount of ultraviolet light-induced defect sites.

Figure 11 shows the relationship between the contact angle, calcined time, and wetting time for a water droplet added to the surface, for porous TiO_2 thin films have been heat-treated at 450 °C for various times. It can be seen that the water contact angle decreased with the wetting time for a water droplet added to the surface time for the same heat treatment time of porous TiO_2 thin films. On the other hand, the water contact angle decreased rapidly and was saturated at 34.4°, 5.0°, and 2.0°, when heat-treated at 450 °C for 10, 30, and 60 min, respectively. This result, ascribed to the heat treatment time increasing from 10 to 60 min, enhanced the crystallinity of anatase TiO_2, which created the defect sides of (100) and (110) reflections on the surface of porous TiO_2 thin films. This result increases the amount of the ultraviolet light irradiated. The surface wettability conversion greatly depends on the amount of light-induced defect sites that are relevant to the surface structure of the TiO_2 crystal [52].

As mentioned above, the superhydrophilic properties of TiO_2 porous thin films without UV light radiation can be obtained for thin films that are first fabricated by a sol–gel spin-coating process and, subsequently, for TiO_2 thin films after suitable heat treatment.

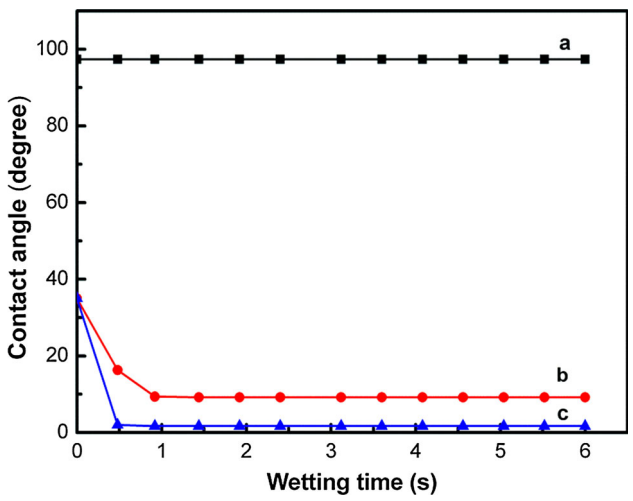

Fig. 10 Dependence of contact angle on heat treatment temperature and wetting times for a water droplet added to the surface: *a* 300 °C; *b* 400 °C; and *c* 450 °C

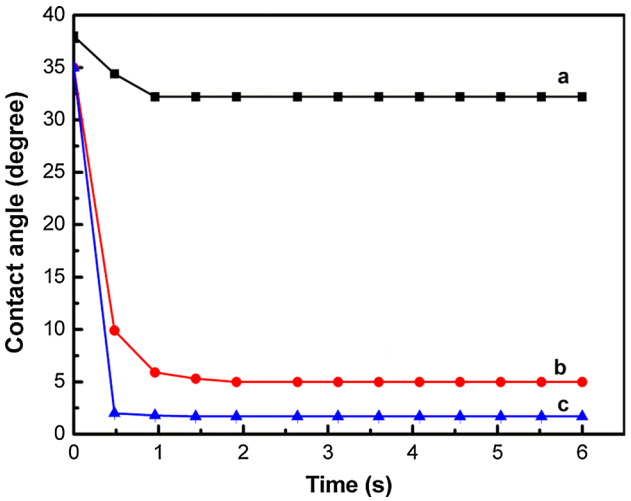

Fig. 11 Relationship between contact angle, calcined time, and wetting time added to surface of porous TiO_2 thin films after heat treatment at 450 °C for various times: *a* 10 min; *b* 30 min; and *c* 60 min

4 Conclusion

TiO_2 porous thin films were fabricated successfully using $Ti(OBu)_4$ and absolute ethanol as the initial materials, with AcAc and DEA as the complexing agents, prepared by a sol–gel spin-coating process. The effect of heat treatment on the crystalline structure and hydrophilic properties of TiO_2 porous thin films was investigated by XRD, FTIR, FESEM, and WCA measurements. The conclusions of the present work are summarized as follows:

1. XRD results show that the calcined powders still maintained the amorphous state when the precursor powders had been calcined at 300 and 350 °C for 1 h. In addition, the calcined powders only contained a single phase of anatase TiO_2 when the precursor powders had been calcined at 400–550 °C for 1 h.
2. The TiO_2 thin films revealed the amorphous state after being heat-treated at temperatures between 300 and 400 °C, whereas the thin films contained a single phase of anatase TiO_2 after heat treatment at temperatures between 450 and 550 °C.
3. The size of TiO_2 pore thin films, before and after heat treatment, can be divided into two: 7.28 and 7.96 μm; 4.16 and 4.64 μm, respectively. This result shows that the pore size of TiO_2 thin films was affected by the heat treatment.
4. The TiO_2 thin films, before and after heat treatment, at temperatures lower than 200 °C for 1 h, where the WCA was >96.8°, revealed the hydrophobic property. On the other hand, with heat treatment at temperatures greater than 400 °C for 1 h, the TiO_2 thin films exhibited the hydrophilic property with a WCA smaller than 9.2°.
5. When the TiO_2 porous thin films had been heat-treated at 450 °C for 30 and 60 min, the thin films possessed WCAs smaller than 5° and showed the superhydrophilic property.

Acknowledgments The authors would like to express sincere thanks for the financial support from the Science and Technology Planning Project of Wuhan City (2013010501010135), the Science and Technology Planning Project of Hubei Province (2014BAA136), National Natural Science Foundation of China (51372179), and the Independent Innovation Research Fund of Wuhan University of Technology (20510070).

References

1. Rupp F, Haupt M, Klostermann H, Kim HS, Eichler M, Peetsch A, Scheideler L, Doering C, Oehr C, Wendel HP, Sinn S, Decker E, von Ohle C, Geis-Gerstorfer J (2010) Acta Biomater 6:4566–4577
2. Kesmez Ö, Çamurlu HE, Burunkaya E, Arpaç E (2009) Sol Energy Mater Sol Cells 93:1833–1839
3. Tahk D, Kim T, Yoon H, Choi M, Shin K, Suh KY (2010) Langmuir 26:2240–2243
4. Zhang X, Su H, Zhao Y, Tan T (2008) J Photochem Photobiol A Chem 199:123–129
5. Zhao X, Zhao Q, Yu J, Liu B (2008) J Non Cryst Solids 354:1424–1430
6. Wang R, Hashimoto K, Fujishima A, Chikuni M, Kojima E, Kitamura A, Shimohigoshi M, Watanabe T (1997) Nature 388:431–432
7. Fujishima A, Rao TN, Tryk DA (2000) J Photochem Photobiol C Photochem Rev 1:1–21
8. Yu J, Zhao X, Zhao Q, Wang G (2001) Mater Chem Phys 68:253–259
9. Yu J, Zhao X, Zhao Q (2001) Mater Chem Phys 69:25–29
10. Arconada N, Durán A, Suárez S, Portela R, Coronado JM, Sánchez B, Castro Y (2009) Appl Catal B Environ 86:1–7
11. Wang J, Li H, Li H, Zuo C, Wang H (2012) J Phys Chem C 116:9517–9525
12. Takeda S, Suzuki S, Odaka H, Hosono H (2001) Thin Solid Films 392:338–344
13. Shimizu K, Imai H, Hirashima H, Tsukuma K (1999) Thin Solid Films 351:220–224
14. Okuya M, Nakade K, Kaneko S (2002) Sol Energy Mater Sol Cells 70:425–435
15. Xu K, Zhu G (2009) Appl Surf Sci 255:6691–6695
16. Meher SR, Biju KP, Jain MK (2009) J Solgel Sci Technol 52:228–234
17. Sakai N, Wang R, Fujishima A, Watanabe T, Hashimoto K (1998) Langmuir 14:5918–5920
18. Watanabe T, Nakajima A, Wang R, Minabe M, Koizumi S, Fujishima A, Hashimoto K (1999) Thin Solid Films 351:260–263
19. Houmard M, Riassetto D, Roussel F, Bourgeois A, Berthomé G, Joud JC, Langlet M (2007) Appl Surf Sci 254:1405–1414
20. Qu Y, Song S, Jing L, Luan Y, Fu H (2010) Thin Solid Films 518:3177–3181
21. Xiong J, Das SN, Kim S, Lim J, Choi H, Myoung JM (2010) Surf Coat Tech 204:3436–3442
22. Peng B, Tan L, Chen D, Meng X, Tang F (2012) Appl Mater Interfaces 4:96–101
23. Wang MC, Lin HJ, Yang TS (2009) J Alloys Compds 473:394–400
24. Lopez T, Sanchez E, Bosch P, Meas Y, Gomez R (1992) Mater Chem Phys 32:141–152
25. Huang W, Chen Y, Yang C, Situ Y, Huang H (2015) Ceram Int 41:7573–7581
26. Aparna AR, Brahmajirao V, Kartikeyan TV, Monnesha F (2016) IOSR J Appl Phys 8:18–26
27. Brinkhuis RHG, Schouten AJ (1991) Macromolecules 24:1496–1504
28. Li L, Liu CY (2010) CrystEngComm 12:2073–2078
29. Ramesh S, Leen KH, Kumutha K, Arof AK (2007) Spectrochim Acta 66:1237–1242
30. Kuo CW, Shen YH, Wen SB, Lee HE, Hung IM, Huang HH, Wang MC (2011) Ceram Int 37:341–347
31. Yang GL, Ko HH, Hsu YW, Yang KH, Wang MC, Han J, Zhao XJ (2013) Ceram Int 39:6805–6811
32. Li G, Li L, Boerio-Goates J, Woodfield BF (2005) J Am Chem Soc 127:8659–8666
33. Katoch A, Kim H, Hwang T, Kim SS (2012) J Solgel Sci Technol 61:77–82
34. Yeh SW, Chen YL, Hsi CS, Ko HH, Wang MC (2014) Metall Mater Trans A 45A:261–268
35. Yeh SW, Ko HH, Chiang HM, Chen YL, Lee JH, Wen CM, Wang MC (2014) J Alloys Compds 613:107–116
36. Liao SC, Mayo WE, Pae KD (1997) Acta Mater 45:4027–4040
37. Tonejc AM, Djerdj I, Tonejc A (2001) Mater Sci Eng B 85:55–63

38. Lin HJ, Yang TS, Hsi CS, Wang MC, Lee KC (2014) Ceram Int 40:10633–10640
39. Lin HJ, Yang TS, Wang MC, Hsi CS (2014) J Alloys Compds 610:478–485
40. Paz Y, Heller A (1997) J Mater Res 12:2759–2766
41. Konishi J, Fujita K, Nakanishi K, Hirao K (2006) Chem Mater 18:6069–6074
42. Bu SJ, Jin ZG, Liu XX, Yang LR, Cheng ZJ (2005) J Euro Ceram Soc 25:673–679
43. Huang T, Huang W, Zhou C, Situ Y, Huang H (2012) Surf Coat Technol 213:126–132
44. Nakanishi K, Tanaka N (2007) Acc Chem Res 40:863–873
45. Malfatti L, Bellino MG, Innocenzi P, Soler-Illia GJAA (2009) Chem Mater 21:2763–2769
46. Carn F, Colin A, Achard MF, Deleuze H, Sanchez C, Backov R (2005) Adv Mater 17:62–66
47. Chen Y, Zhang C, Huang W, Yang C, Huang T, Situ Y, Huang H (2014) Surf Coat Technol 258:531–538
48. Nakanishi K (1997) J Porous Mater 4:67–112
49. Situ Y, Huang T, Chen Y, Huang W, Huang H (2014) Ceram Int 40:919–927
50. Nakanishi K, Takahashi R, Nagakane T, Kitayama K, Koheiya N, Shikata H, Soga N (2000) J Solgel Sci Technol 17:191–210
51. Wenzel RN (1936) Ind Eng Chem 28:988–994
52. Wang R, Sakai N, Fujishima A, Watanabe T, Hashimoto K (1999) J Phys Chem B 103:2188–2194